BIOCHEMISTRY
including biophysical chemistry & molecular biology
Article

*Biochemistry* **2009,** *48,* 7849–7855 7849
DOI: 10.1021/bi901003k

# Solution Structures of the Actuator Domain of ATP7A and ATP7B, the Menkes and Wilson Disease Proteins[†,‡]

Lucia Banci,[§,⊥,¶] Ivano Bertini,*[,§,⊥] Francesca Cantini,[§,⊥] Manuele Migliardi,[§] Giovanni Natile,[#] Fiorentin Nushi,[#] and Antonio Rosato[§,⊥]

[§]*Magnetic Resonance Center (CERM) - University of Florence, Via L. Sacconi 6, 50019 Sesto Fiorentino, Italy,* [⊥]*Department of Chemistry - University of Florence, Via della Lastruccia 3, 50019 Sesto Fiorentino, Italy,* [¶]*FIORGEN Foundation, Via L. Sacconi 6, 50019 Sesto Fiorentino, Italy, and* [#]*Department Farmaco-Chimico - University of Bari "Aldo Moro" - Via E. Orabona 4, 70125 Bari, Italy*

*Received June 15, 2009; Revised Manuscript Received July 21, 2009*

ABSTRACT: ATP7A and ATP7B are two human $P_{1B}$-type ATPases that have a crucial role in maintaining copper(I) homeostasis. Among the various domains of these enzymes, one, called the Actuator or A-domain, has a regulatory function and is required for the phosphatase step of the catalytic cycle (dephosphorylation of the intermediate formed during ATP hydrolysis). Here we report the solution structures of the A-domain of both proteins, solved by heteronuclear NMR spectroscopy and a characterization of the dynamics of the A-domain of ATP7A. We observed that the catalytically important TGE loop protrudes from the structure ready for interaction with the phosphorilated site in the ATP-binding domain. The loop is rigid, suggesting that the catalytic step does not require substantial structural flexibility or rearrangements. The present structures were useful to rationalize the molecular effects of disease-causing mutations. In particular, it can be concluded that mutations occurring in the A-domain either destabilize the fold of the domain (such as Gly860Val in ATP7A) or affect the network of communication within the domain (such as Leu873Arg in ATP7A) or with the other domains of the enzyme (such as Gly853Arg in ATP7A).

Copper plays an important role as cofactor of redox proteins, but at the same time it can also participate in vivo in redox reactions generating harmful highly reactive oxidative species (*1*, *2*) and interacting with protein ligands (*3*). For this reason copper uptake, distribution, and excretion must be tightly controlled. One of the pathways that regulate copper transfer and homeostasis in humans involves HAH1, a small soluble metallochaperone (*4*), which is capable of delivering copper(I) to both the ATP7A (Menkes or MNK) and ATP7B (Wilson or WLN) proteins. The latter belong to the subfamily of $P_{1B}$-type ATPases and couple ATP hydrolysis with the transport of copper(I) across membranes (*5*−*7*). Under low copper conditions, they shuttle copper to the secretory pathway of the trans Golgi network (TGN), where the metal ion is incorporated into copper-dependent enzymes (*8*). An increase of the intracellular copper concentration results in the trafficking of the ATP7A and ATP7B proteins to the plasma membrane in order to efflux copper out of the cell (*9*−*11*).

In humans, mutations in the ATP7A and ATP7B genes cause improper function of these copper(I)-ATPases, leading to severe inheritable diseases that involve dysfunctional copper homeostasis, named Menkes and Wilson diseases (MD and WD), respectively (*12*, *13*). MD is a fatal X-linked copper deficiency disorder having multiple abnormalities that can be related to deficiencies in cuproenzymes (*12*). Affected patients usually die in early childhood. In WD, very high concentrations of copper are accumulated in the liver because the biliary excretion of the metal ion is defective. If the disease is not treated, death can result from liver failure.

All P-type ATPases share a basic "core" architecture (*14*) comprising a hydrophilic region protruding into the cytosol, which contains the phosphorylation and the ATP-binding sites (P- and N-domains, respectively) and a smaller region (called the Actuator or A-domain), which has a regulatory function and is required for the phosphatase step of the catalytic cycle (dephosphorylation of the intermediate formed during ATP hydrolysis). These cytosolic parts of the polypeptide chain are connected by a number of transmembrane helices, which are involved in the formation of an intramembranous channel, and whose organization leads to the definition of the P1 and P2 subgroups (*15*). In addition to the core structure, a distinguishing feature of $P_{1B}$-type copper(I)-transporting ATPases is their long N-terminal tail, which contains a variable (between one and six) number of 70-aa independently folded copper(I)-binding domains (*15*). The transmembrane region of $P_{1B}$-type ATPases is formed by eight transmembrane helices (TMHs). The P- and N-domains are located between the sixth and the seventh TMH, whereas the A-domain is located between the fourth and the fifth TMHs.

The ion-translocation cycle of $P_{1B}$-type ATPases has been proposed to follow the E1/E2 Post-Albers catalytical cycle (*16*, *17*) (Figure 1, which has been originally proposed for $P_2$-ATPases ($Na^+$,$K^+$-, $Ca^{2+}$- and $H^+$,$K^+$-transporting ATPases). The initial steps in the catalytic cycle are the binding of ATP to

[†]Financial support from MIUR (FIRB project no. RBLA032ZM7), Ente Cassa di Risparmio di Firenze (Project "Relazione varianti proteiche strutturali-malattie genetiche"), and the European Commission (Project SPINE2-COMPLEXES-No. 031220) is gratefully acknowledged.

[‡]Resonance assignments and the final atomic coordinates of A-MNK, with all the restraints used in calculations, are available at the BioMagResBank (16277) and at the Protein Data Bank (2kij), respectively.

*Corresponding author. Fax: +39 055 4574271. Tel: +39 055 4574272. E-mail: ivanobertini@cerm.unifi.it.


Published on Web 07/31/2009

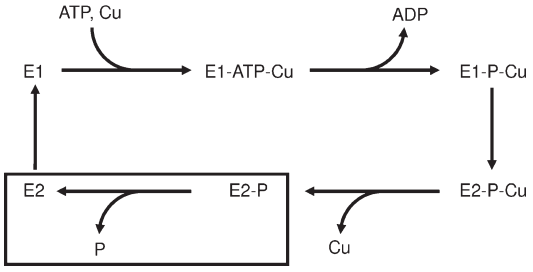


FIGURE 1: A simplified catalytic cycle of Cu-ATPases based on the Post-Albers scheme. The step in which the A-domain is involved is highlighted with the black box.

the N-domain and metal ion binding to the TM region (E1 state). Subsequently, a transient phosphorylated intermediate is formed upon transfer of the $\gamma$-phosphate from ATP to the invariant Asp residue of the DKTG motif located in the P-domain, leading to the occlusion of the metal within the TM region (E1P state). A successive conformational change allows the metal ion to be released on the other side of the membrane (E2P state); then, the dephosphorylation reaction occurs (E2 state). The latter step of the cycle is performed by the TGE motif present in the A-domain. From the E2 state, the enzyme progresses to the E1 state and another cycle can start. During the various steps of the catalytic cycle the N-, P-, and A-domains undergo large relative movements, which are coupled to rearrangements of the position of the TMHs (*18*).

In the present work, we characterized the structure and dynamics in solution of the actuator domain of both ATP7A and ATP7B (hereafter referred to as A-MNK and A-WLN respectively), in order to investigate how these properties are related to the functional properties of these domains. Moreover, the present structures provide hints on the consequences at the molecular level of the pathogenic missense mutations leading to Menkes and Wilson diseases.

## MATERIALS AND METHODS

*Protein Expression and Purification*. The DNA segment encoding the A-domain of ATP7A, corresponding to amino acids 806−924 of ATP7A, was amplified via PCR from human cDNA and cloned in the Gateway Entry vector pENTR/TEV/D-TOPO (Invitrogen) to include the TEV protease cleavage site at the N-terminal end. This segment was then subcloned into pETG-20A (EMBL-Heidelberg) through the Gateway LR reaction, yielding a plasmid expressing the protein fused with Thioredoxin-A and a His tag at the N terminus. After cleavage of the tag, five amino acids from the restriction site are left at the N-terminus of the protein. The same procedure was followed to clone the A-domain of ATP7B (residues 789−907). *Escherichia coli* strain BL21(DE3) Gold (Stratagene) was used for protein expression. Cells were grown at 25 °C for 16 h in minimal media cultures. For isotope enrichment, $(^{15}NH_4)_2SO_4$ and $^{13}$C-glucose were used. The two proteins were purified by using the HisTrap chelating FF column (GE Healthcare) followed by an anionic exchange step performed using a 16/10 Q FF column (GE Healthcare). After this, the His tag was cleaved with AcTEV protease (Invitrogen) and removed applying the protein samples again onto the affinity column. Proteins purity was checked by SDS−PAGE and matrix-assisted laser desorption ionization time-of-flight mass spectra. The normal yield of both proteins was 20 mg/L. Uncleaved proteins could be stored for months at −80 °C.

*NMR Sample Preparation*. NMR samples contained between 0.2 and 0.3 mM protein in 50 mM phosphate, 50 mM arginine, 50 mM glutamate at pH 7.0. Because of the presence of a cysteine residue in A-MNK, the samples were reduced with excess of DTT and manipulated in an inert atmosphere chamber (Coy Lab). NMR samples contained 10% (v/v) $^2H_2O$ for NMR spectrometer lock.

*NMR Experiments and Structure Calculations*. NMR spectra were acquired at 298 K on Avance 900, 700, and 500 Bruker spectrometers equipped with triple resonance cryoprobes. The NMR experiments used for the assignment of backbone and aliphatic side chain resonances of both A-MNK and A-WLN domains are summarized in Supporting Information (SI) Table S1. Resonance assignments of the two domains are reported as SI (Tables S2 and S3). Backbone dihedral angle constraints were derived from $^{15}$N,$^{13}$C',$^{13}$C$\alpha$,$^{13}$C$\beta$, and H$\alpha$ chemical shifts, using TALOS (*19*). Distance constraints for structure determination were obtained from $^{15}$N-edited and $^{13}$C-edited 3D NOESY-HSQC spectra. For A-MNK one-bond $^1$H−$^{15}$N dipolar couplings were measured in samples containing 11 mg/mL of Pf1 bacteriophage (ASLA, Ltd., Latvia) at 800 MHz by using the in-phase/antiphase method (*20*, *21*).

For A-MNK 500 random conformers were annealed in 10 000 steps using the program CYANA-2.1 (*22*). For residual dipolar coupling restraints, the alignment tensor parameters were obtained with FANTAORIENT, and they were optimized through iterative cycles of PSEUDOCYANA until convergence (*23*).

For A-WLN we applied an automated method for structure calculation, based on the ATNOS/CANDID algorithms (*22*, *24*) for NOESY peak picking and assignment, implemented in the UNIO package (http://perso.ens-lyon.fr.hermann/Hermann/Software.html). A structural model of the A-WLN domain, built on the average NMR structure of A-MNK as the template, was used as input to the first ATNOS/CANDID cycle to produce an initial list of upper distance restraints to be passed on to the subsequent CYANA-2.1 calculation cycle.

The 30 conformers with the lowest residual target function values of both A-MNK and A-WLN domains were subjected to refinement with the AMBER 10.0 package (*25*) in explicit water. NOE and torsion angle constraints were applied with force constants of 50 kcal mol$^{-1}$ Å$^{-2}$ and 32 kcal mol$^{-1}$ radians$^{-2}$, respectively. The conformational and energetic analysis together with selected quality parameters from PROCHECK-NMR, WHATIF analysis, and Protein Structure Validation Software (PSVS) suite (*26*−*28*) of the final family of A- MNK is reported in table S4. The program MOLMOL was used for structure analysis (*29*). After energy minimization in explicit solvent, the final bundle of 30 conformers of A-MNK had an average target function of 1.15 ± 0.13 Å$^2$ (CYANA units). The average backbone RMSD value, (over residues 2−118) was 0.92 ± 0.18 Å. The final bundle of 30 conformers of A-WLN had an average target function of 1.74 ± 0.57 Å$^2$ (CYANA units) and the average backbone RMSD value (over residues 2−118) was 0.94 ± 0.07 Å.

*Structure Modeling*. For the analysis of residue conservation, we used the full sequence of ATP7A as input to the BLAST program (*30*), and aligned the best 200 hits with CLUSTALW (*30*, *31*). The structure of the ATP-domain of ATP7A and ATP7B were modeled using as template the structure of corresponding domain of the homologous protein from *A. fulgidus* (PDB code 2B8E) (*32*), using the program Modeler V. 9.1 (*33*).

*NMR Mobility Data Acquisition and Analysis*. The dynamic properties of A-MNK have been directly sampled

through $^{15}N$ relaxation measurements. $^{15}N$ longitudinal and traverse relaxation rates (*34*) and $^{15}N\{^1H\}$-NOEs (*35*) were recorded at 500 MHz, using a protein concentration of 0.3 mM. $R_1$ and $R_2$ relaxation rates were obtained by fitting the cross peak volumes (I), measured as a function of the relaxation delay, to a single exponential decay as described in the literature (*36*). Heteronuclear NOE values were calculated as the ratio of peak volumes in spectra recorded with and without saturation. In all experiments the water signal was suppressed with the "water flipback" scheme (*35*). The average backbone $^{15}N$ longitudinal $R_1$ and transversal $R_2$ relaxation rates and $^{15}N\{^1H\}$-NOEs values of A-MNK are 1.8 ± 0.1 $s^{-1}$, 11.3 ± 2.3 $s^{-1}$, and 0.64 ± 0.04 (Figure S1A−C, Supporting Information). The relaxation data ($R_1$, $R_2$, and $^{15}N\{^1H\}$-NOEs) were analyzed according to the model-free approach of Lipari and Szabo (*37*, *38*), using the program TENSOR2 (*18*).

## RESULTS AND DISCUSSION

*A-MNK Structure Determination and Comparison with A-WLN*. The cloned constructs of the A-domains of the ATP7A and ATP7B proteins correspond to amino acids 806−924 and 789−907 of ATP7A and of ATP7B, respectively. Both protein constructs, referred to as A-MNK and A-WLN, are of the same length. For the sake of simplicity, residues are here numbered from 1 to 119 (not taking into account the five aminoacids engineered expression tag located at the N-terminus). In this scheme, corresponding residues of A-MNK and A-WLN have the same number.

Good quality NMR spectra for both A-MNK and A-WLN were obtained by using a 50 mM phosphate buffer at pH 7.0 that contained also 50 mM arginine and 50 mM glutamate (*39*). The protein concentration was 0.3 mM. We assigned all the amide moieties of A-MNK, with the sole exceptions of Glu2 and Thr107. For A-WLN, all residues were assigned, except Glu2, Ala12, Thr13, and Thr107.

The solution structure of A-MNK (Figure 2) is characterized by seven antiparallel $\beta$-strands ($\beta$3 (44−45), $\beta$4 (56−58), $\beta$5 (62−65), $\beta$6 (76−77), $\beta$7 (82−85), $\beta$8 (89−90), $\beta$9 (95−99)) that are arranged in two sheets (comprising $\beta$3, $\beta$4, $\beta$7, and $\beta$9, and $\beta$5, $\beta$6, and $\beta$8, respectively) packed against each other. These two sheets form a distorted double-stranded beta-helix fold. Two additional $\beta$-strands ($\beta$1 (13−20) and $\beta$2 (28−33)) form a $\beta$-hairpin structure flanking the two sheets. Finally, two helices (α1 (2−10), α2 (107−117)), which are the cytosolic extension of the fourth and fifth TMHs of the enzyme, are present at the N- and C- termini of the structure. Figure 2 shows that the secondary structure elements are well ordered; only a few residues in the loop regions feature some local disorder.

The core of the protein is characterized by hydrophobic interactions between aliphatic residues located on the first sheet and aliphatic as well as aromatic residues located on the other sheet. In addition, the aliphatic side chains of residues Leu68, Ile69 (Loop 6), Ile85 (strand $\beta$7), and Ala86 form hydrophobic interactions with aliphatic residues belonging to the two α-helices; the latter interactions determine the position of the helices with respect to the rest of the protein, which in calculations is defined also thanks to the residual dipolar coupling restraints (Figure S2, Supporting Information).

The structure of A-WLN (Figure 3B and ,Figure S3, Supporting Information), which was automatically calculated, is very similar to that of A-MNK, the average backbone RMSD between the two being 1.6 Å. This is in agreement with their high sequence identity (> 80%, Figure 4). The secondary structure elements are similar in length and in the spatial orientation. Furthermore, all hydrophobic contacts involving conserved aliphatic and aromatic residues, which are crucial to determine the fold of the protein, are conserved in both solution structures.

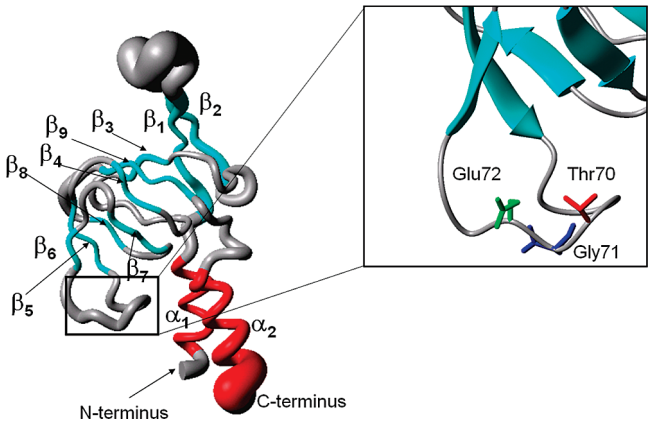


FIGURE 2: Solution structure of A-MNK (residues 1−119). The radius of the tube is proportional to the backbone RMSD of each residue. The secondary structure elements are shown: $\beta$-strands are shown in cyan and helices in red. The α-helices and the $\beta$-strands are labeled. In the inset the side chains of the residues of the TGE sequence motif are shown.

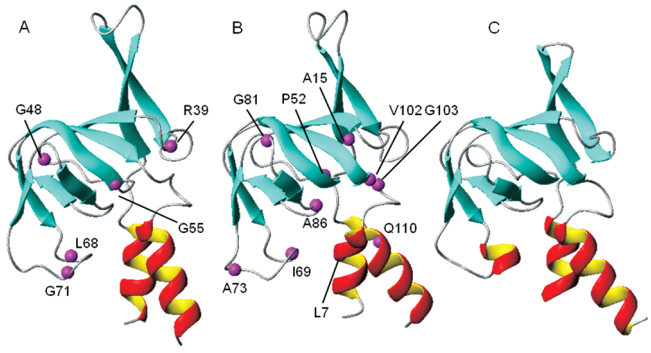


FIGURE 3: Ribbon diagram of A-domains. Comparison of the A-MNK (A), A-WLN (B), and A-domain from *A. fulgidus* (PDB ID 2HC8) (C). A-MNK and A-WLN pathogenic missense mutations are shown as magenta-colored spheres.

*A-MNK Dynamics*. The dynamics of A-MNK was investigated by performing $^{15}N$ relaxation measurements at 298 K. The correlation time for protein tumbling ($\tau_m$) was estimated from the $R_2/R_1$ ratios and was found to be 9.1 ± 0.7 ns, which is consistent with a protein being in a monomeric state; the value predicted by the HYDRONMR program (*40*) was 8.96 ns.

The order parameters $S^2$, obtained from the analysis of the $^{15}N$ relaxation data, are shown in Figure S1D, Supporting Information. Some protein dynamics in the sub-nanosecond time scale is observed for the C-terminus. Within the folded part of the polypeptide chain, mobile regions are essentially all located in loops connecting secondary structure elements, including the $\beta$-hairpin loop. The most mobile region corresponds to the loop between strands $\beta$8 and $\beta$9, with $S^2$ values between 0.7 and 0.8 for residues 92−95. Thus, the structure of A-MNK is overall quite ordered, with little dynamics affecting both the secondary structure regions as well as the loop regions (excluding the C-terminus).

*Comparison with Other ATPases*. The only available three-dimensional structure of the actuator domain of a

```
                  α1 α1 α1 α1 α1 α1 α1 α1 α1     β1 β1 β1 β1 β1 β1 β1 β1          β2 β2 β2 β2 β2          β3 β3 β3                    β4 β4 β4
A-MNK      1  S E A L A K L I S L Q A T E A T I V T L D S D N I L L S E E Q V D V E L V Q R G D I I K V V P G G K F P V D G R V I E     59
A-WLN      1  S E A L A K L M S L Q A T E A T V V T L G E D N L I I R E E Q V P M E L V Q R G D I V K V V P G G K F P V D G K V L E     59
A-Dom      1  - E A I K K L V G L Q A K T A V V I R D G - - - - - - K E I A V P V E E V A V G D I V I V R P G E K I P V D G V V V E     52
A. Fulgidus

                  β5 β5 β5 β5                  β6 β6 β6 .        β7 β7 β7 β7       β8 β8 β8       β9 β9 β9 β9 β9          α2 α2 α2 α2 α2 α2 α2 α2 α2 α2
A-MNK     60  G H S M V D E S L I T G E A M P V A K K P G S T V I A G S I N Q N G S L L I C A T H V G A D T T L S Q I V K L V E E A Q -  119
A-WLN     60  G N T M A D E S L I T G E A M P V T K K P G S T V I A G S I N A H G S V L I K A T H V G N D T T L A Q I V K L V E E A Q -  119
A-Dom     53  G E S Y V D E S M I S G E P V P V L K S K G D E V F G A T I N N T G V L K I R A T R V G G E T L L A Q I V K L V E D A M G  113
A. Fulgidus
```

FIGURE 4: Sequence alignment of A-MNK, A-WLN, and A-domain from *A. fulgidus*. The secondary structure elements of A-MNK are shown.

copper-transporting ATPase homologous to the human ones studied here is that of the enzyme from *Archaeoglobus fulgidus* (PDB code 2HC8) (*32*). The structures of A-MNK and A-WLN have a backbone rmsd to the 2HC8 structure of about 1.8 Å, while the corresponding sequence identity is on average 62% (Figure 4). As shown in Figure 3A−C, the three structures contain the same elements of secondary structure, with very similar relative orientations. It is to be noted that the chemical shift index (*41*) indicates that the A-MNK and A-WLN structures contain nine $\beta$-strands, whereas 2HC8 has been described as having 10 strands (*32*). However, the calculation of secondary structure elements with the program PROCHECK (*42*) using the deposited coordinates of 2HC8 indicates that residues 255−257, reported to form strand $\beta$4, do not feature a regular secondary structure. This analysis can be performed online at http://www.ebi.ac.uk/thornton-srv/databases/cgi-bin/pdbsum/RunPROCHECK.pl?pdb=2hc8.

From multiple sequence alignments of the actuator domain of copper-transporting ATPases, it appears that an insertion is present in eukaryotic with respect to the large majority of prokaryotic organisms in the $\beta$-hairpin loop (i.e., between strands $\beta$1 and $\beta$2). With respect to the *A. fulgidus* protein, this insertion comprises six amino acids, residues 22−27 (Figure 3). Even though this loop is solvent exposed, the insertion contains two or three nonpolar amino acids, for example, Ile-Leu-Leu and Leu-Ile-Ile in A-MNK and A-WLN, respectively (Figure 4). On the basis of the low-resolution structure of the entire *A. fulgidus* enzyme solved by cryoelectron microscopy (*43*), it appears that this loop is well positioned to interact with the long N-terminal tail. The latter contains up to six metal-binding domains in eukaryotic proteins, whereas it contains typically one or two domains in prokaryotic proteins. In the latter systems, the tail would presumably be too short to permit contacts with the region of the A-domain in object, hence its shorter loop. The long eukaryotic tail has been proposed to serve a regulatory role (*44*), and the interaction with the 22−27 loop might be instrumental for the communication between the N-terminal tail and the other cytosolic domains, presumably in a copper-dependent manner.

Various regions in the actuator domain are important for enzyme function, because of their interaction with the other domains of the protein. The TGE sequence motif plays a crucial role in the catalytic cycle of copper-transporting ATPases. The Gly and Glu amino acids of the TGE motif are conserved in all organisms, whereas the Thr is sometimes conservatively substituted by Ser. The Glu residue (Glu72 in these structures) is required for the dephosphorylation of the E2P intermediate, thus leading to E2. Its side chain appears to provide general base catalysis by abstracting a proton from a water molecule brought into the correct position by the backbone carbonyl of the Thr70 residue (*45*). To perform this function, Glu72 must protrude toward the conserved Asp in the conserved DKTGT motif that

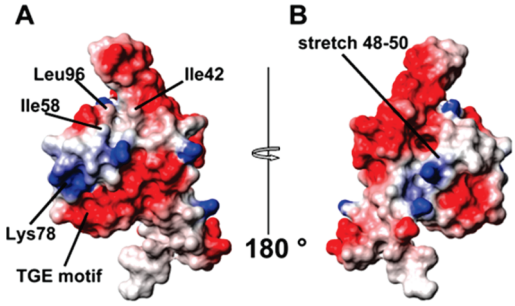


FIGURE 5: Electrostatic surface of A-MNK. Areas of negative, positive, and neutral electrostatic potential are depicted in red, blue, and white, respectively. The conserved TGE motif and the residues believed to interact with the P-domain are indicated. The position of some residues possibly involved in interactions with other domains is also indicated.

constitutes the phosphorylation site within the P domain (*45*). In A-MNK, the loop region containing the TGE motif is rather rigid with an average $S^2$ value for backbone amides of 0.91 ± 0.05. This region is quite ordered in the structure, and the side chain of Glu72 is oriented toward the solvent. Notably, when comparing the structures of the related SERCA calcium-transporting P-type ATPase solved in states that represent the various intermediates along the catalytic cycle (*45*, *46*), it can be observed that this loop undergoes only minor structural rearrangements for the protein backbone, essentially limited to the Glu72 residue. The presently observed rigidity of the TGE loop in A-MNK suggests that this behavior may be common also to copper(I)-transporting ATPases. The electrostatic potential around the TGE motif is quite negative (Figure 5), due to the presence not only of the conserved Glu72 but also of Asp54 and Glu66. These residues are conserved in both prokaryotic and eukaryotic copper-transporting ATPases.

Cross-linking experiments on the *Enterococcus hirae* copper-transporting ATPase (*47*) indicated that also the region 79−81 is involved in interactions with the P-domain, via Lys79. This residue is not particularly conserved; nevertheless, residue 78 is a conservatively substituted Lys, again suggesting that the electrostatic potential (Figure 5) in this region is important for interaction with the P-domain.

Another functionally important region involves residues 48−50, which in SERCA are involved in interdomain interactions with residues in the seventh α-helix of the P-domain (*48*). Gly48, in particular, is strictly conserved and lies within a relatively nonpolar region of the surface (Figure 5); residue 49 is variable, whereas Lys50 is present in the large majority of the sequences or is otherwise often conservatively substituted by Arg. The region of the P-domain interacting with the stretch 48−50 has a negative electrostatic potential, thus complementary to the charge of the Lys side chain (Figure S4, Supporting Information).

Three aliphatic residues of A-MNK and A-WLN (Ile42, Ile58, and Leu96), which are conserved in copper-transporting ATPases as well as in the SERCA ATPase, form a solvent-exposed hydrophobic region on the $\beta$-sheet comprising strands $\beta$3, $\beta$4, $\beta$7, and $\beta$9 (Figure 5). The actuator domain of SERCA contains an additional (with respect to $P_{1B}$-type ATPases) N-terminal subdomain (dubbed A1). In SERCA, the above-mentioned hydrophobic region constitutes part of the interface with the A1 subdomain, and the latter has a critical role in transmitting to the membrane region the movement of the A-domain relative to the P domain, directly affecting the orientation of the TMHs (*45*, *49*). Papain digestion studies performed on the copper-transporting ATPase CopA from *Thermotoga maritima* in various functional states (*50*) has suggested that the N-terminal soluble metal binding domain (MBD) interacts with the smaller A-domain of $P_{1B}$-type ATPases, forming an unit that could be functionally equivalent to the entire A-domain of SERCA. The structural model of the copper-transporting ATPase CopA from *E. hirae* obtained by cross-linking experiments (*47*) is in agreement with this model.

*A-MNK and A-WLN Mutations*. Eight A-MNK mutations leading to Menkes disease have been reported in the Human Gene Mutation Database, HGMD, at http://www.hgmd.org. Three of them (Gln11-term, Gln91-term, and Gln119-term) result in truncation of the protein, while five are missense mutations (Arg39His, Gly48Arg, Gly55Val, Leu68Arg, and Gly71Arg or Glu) (Figure 3A). The latter residues are conserved in the A-domains of copper $P_{1B}$-type ATPases, with the exception of Arg39 and of Leu68. The latter is however conservatively substituted by a Met or Phe hydrophobic residue. Note that the above numbering refers to the present construct and can be transformed into the numbering of full-length ATP7A by adding 805.

The present structures are fundamental to provide some hints on the structural consequences of the pathogenic missense mutations. Gly48 is located in a well-structured, quite rigid loop connecting strands $\beta$3 and $\beta$4 and, as mentioned above, in SERCA is part of the region involved in the interaction with P-domain (*48*). The mutation of Gly48 into Arg would presumably determine a variation of the conformation of the loop, due to both the large volume of the side chain and to the charge−charge repulsion that would occur with Lys50, adversely affecting the interaction with the P domain.

Gly55 is located at the N-terminus of the strand $\beta$4. Its mutation into Val would destabilize the structure of the $\beta$-sheet due to the steric hindrance, particularly involving the side chain of Ile97, which is part of the hydrophobic core located between the two sheets. Notably, the latter residue is conserved in copper-transporting ATPases but is instead a Gly in SERCA, whereas the residue corresponding to Gly55 is Ile.

Leu68 forms hydrophobic interactions that are important to position the two α-helices with respect to the rest of the protein. The two α-helices in turn are important to transmit the motion of the A-domain to the transmembrane domain of the enzyme (*48*). The mutation of Leu to Arg would disrupt the network of interactions between different regions of the protein and thus impair the communication with the transmembrane domain.

Gly71 is part of the conserved and functional TGE motif of A-domain, and its mutation into Arg or Glu would drastically affect the conformation and thus the role in the enzymatic mechanism as a general base catalysis of Glu72, because of the steric and electrostatic interactions of the latter with the bulky, charged side chains of the mutants.

It is not obvious in the light of the present structure how to rationalize the effect of the Arg39His mutation. Possibly, its adverse effect could be linked to the variation of the electrostatic potential at the surface of A-MNK, which in turn could affect the interaction of this domain with the other cytoplasmatic domains of ATP7A or with molecular partners.

A larger number of disease-causing missense mutations have been reported within A-WLN (Figure 3B). These involve Leu7 (to Arg or Phe), Ala15 (to Thr), Pro52 (to Leu), Ile69 (to Thr), Ala73 (to Thr), Gly81 (to Arg or Val), Ala86 (to Val), Val102 (to Met), Gly103 (to Val), and Gln110 (to Arg). Note that this numbering refers to the present construct and can be transformed into the numbering of full-length ATP7B by adding 788. With the exception of Ala73, Gly81, and Gln110, these mutations involve amino acids that are either in the hydrophobic core of the protein or involved in the contacts among aliphatic (and aromatic) side chains that define the position of the helices with respect to the double stranded $\beta$-helix fold of the core of protein. It is thus conceivable that their mutation impacts adversely on the function of the enzyme by altering the network of communication between the different regions of the protein, which is crucial for the proper progress of the catalytic cycle. Instead, mutations in the hydrophobic core presumably destabilize the fold of the protein.

Ala73 is next to the conserved Glu72, which, as was already mentioned, plays an essential role for the phosphatase activity of the A-domain. Its mutation to Thr, although apparently minor, could in fact affect the positioning of the loop with respect to the P-domain, for example, because of the presence of an additional group that can act both as a donor or acceptor of hydrogen bonds. The hydrogen bond network at the interface of the A- and P-domains is indeed known to be important to define the arrangement of the water molecule that acts as a nucleophile and of the side chain of Glu72 (*45*).

Gly81 is a solvent-exposed residue that is conserved in the large majority (over 90%) of the sequences of ATP7A/B homologues from both eukaryotic and prokaryotic organisms. As described, it is in a region interacting with the P-domain, as found by cross-linking experiments on the *Enterococcus hirae* copper-transporting ATPase (*47*). Its mutation in a longer side chain residue could affect this interaction.

Finally, Gln110 is a solvent-exposed residue that is not known to be involved in interdomain or intermolecular interactions. The impact of the Gln110Arg mutation is not evident from the present structure.

## CONCLUSIONS

We characterized the structures of A-MNK and A-WLN in solution and compared them to the structures of A-domains from other metal-transporting P-type ATPases. In the A-MNK and A-WLN structures, the TGE motif, which is required for the dephosphorylation of E2P intermediate, was properly oriented for the interaction with the P-domain; in particular the side chain of Glu72 protruded into the solvent. We observed that the TGE loop did not experience significant dynamics of the subnanosecond time scale and is thus effectively preorganized for interdomain interactions.

The present structures allowed us to examine the possible mechanisms by which missense mutations in either A-MNK or A-WLN can adversely affect the enzyme activity eventually leading to, respectively, Menkes or Wilson diseases. The mutations can be broadly divided in two groups, one including

residues that are buried within the protein interior, the other including residues located in regions possibly involved in interdomain interactions. The first group of mutations (e.g., in A-MNK, Gly55Ile or Leu68Arg) can influence the function of the enzyme by altering the fold of the domain or by impairing the network of communication between its different regions, and particularly between the TGE motif and the helices. The second group of mutations (e.g., in A-MNK, Gly48Arg, or Gly71Arg/Glu) can impact the phosphatase activity of the A-domain also by altering its interaction with the other cytosolic domains of the enzyme. These results highlighted the importance of the transmission of the effect of molecular events such as substrate binding within and among the various domains of copper(I)-transporting ATPases.

## ACKNOWLEDGMENT

We thank Mr. Stefano Frasca for preparing some protein samples used in initial experiments.

## SUPPORTING INFORMATION AVAILABLE

Four figures which report the relaxation data of A-MNK, the residual dipolar coupling restraints for A-MNK, the structure of A-WLN and the electrostatic potential surface of ATP domain. Four tables reporting the acquisition parameters of NMR experiments, the $^{1}H$, $^{15}N$ and $^{13}C$ resonance assignments of A-MNK and A-WLN and Statistical analysis of the energy minimized family of conformers of A-MNK. This material is available free of charge via the Internet at http://pubs.acs.org.

## REFERENCES

1. Linder, M. C. (1991) Biochemistry of Copper, Plenum Press, New York.
2. Vulpe, C. D., and Packman, S. (1995) Cellular copper transport. *Ann. Rev. Nutr. 15*, 293–322.
3. Koch, K. A., Pena, M. M. O., and Thiele, D. J. (1997) Copper-binding motifs in catalysis, transport, detoxification and signaling. *Chem. Biol. 4*, 549–560.
4. Pufahl, R. A., Singer, C. P., Peariso, K. L., Lin, S.-J., Schmidt, P. J., Fahrni, C. J., Cizewski Culotta, V., Penner-Hahn, J. E., and O'Halloran, T. V. (1997) Metal ion chaperone function of the soluble Cu(I) receptor Atx1. *Science 278*, 853–856.
5. Lutsenko, S., and Kaplan, J. H. (1995) Organization of P-type ATPases: significance of structural diversity. *Biochemistry 34*, 15607–15613.
6. Solioz, M., and Vulpe, C. D. (1996) CPx-type ATPases: a class of P-type ATPases that pump heavy metals. *Trends Biochem. Sci. 21*, 237–241.
7. Axelsen, K. B., and Palmgren, M. G. (1998) Evolution of substrate specificities in the P-type ATPase superfamily. *J. Mol. Evol. 46*, 84–101.
8. Yuan, D. S., Stearman, R., Dancis, A., Dunn, T., Beeler, T., and Klausner, R. D. (1995) The Menkes/Wilson disease gene homologue in yeast provides copper to a ceruloplasmin-like oxidase required for iron uptake. *Proc. Natl. Acad. Sci. U.S.A. 92*, 2632–2636.
9. Petris, M. J., Mercer, J. F., Culvenor, J. G., Lockhart, P., and Camakaris, J. (1996) Ligand-regulated transport of the Menkes copper P-type ATPase efflux pump from the Golgi apparatus to the plasma membrane: a novel mechanism of regulated trafficking. *EMBO J. 15*, 6084–6095.
10. Schaefer, M., Hopkins, R. G., Failla, M. L., and Gitlin, J. D. (1999) Hepatocyte-specific localization and copper-dependent trafficking of the Wilson's disease protein in the liver. *Am. J. Physiol. 276*, G639–G646.
11. La Fontaine, S., and Mercer, J. F. (2007) Trafficking of the copper-ATPases, ATP7A and ATP7B: role in copper homeostasis. *Arch. Biochem. Biophys. 463*, 149–167.
12. Mercer, J. F. (2001) The molecular basis of copper-transport diseases. *Trends Mol. Med. 7*, 64–69.
13. Strausak, D., Mercer, J. F., Hermann, H. D., Stremmel, W., and Multhaup, G. (2001) Copper in disorders with neurological symptoms: Alzheimer's, Menkes, and Wilson diseases. *Brain Res. Bull. 55*, 175–185.
14. Kuhlbrandt, W. (2004) Biology, structure and mechanism of P-type ATPases. *Nat. Rev. Mol. Cell Biol. 5*, 282–295.
15. Arguello, J. M., Eren, E., and Gonzalez-Guerrero, M. (2007) The structure and function of heavy metal transport P1B-ATPases. *Biometals 20*, 233–248.
16. Post, R. L., Hegyvary, C., and Kume, S. (1972) Activation by adenosine triphosphate in the phosphorylation kinetics of sodium and potassium ion transport adenosine triphosphatase. *J. Biol. Chem. 247*, 6530–6540.
17. Albers, R. W. (1967) Biochemical aspects of active transport. *Annu. Rev. Biochem. 36*, 727–756.
18. Dosset, P., Hus, J. C., Marion, D., and Blackledge, M. (2001) A novel interactive tool for rigid-body modeling of multi-domain macromolecules using residual dipolar couplings. *J. Biomol. NMR 20*, 223–231.
19. Schleucher, J., Schwendinger, M., Sattler, M., Schmidt, P., Schedletzky, O., Glaser, S. J., Sørensen, O. W., and Griesinger, C. (1994) A general enhancement scheme in heteronuclear multidimensional NMR employing pulsed field gradients. *J. Biomol. NMR 4*, 301–306.
20. Ottiger, M., Delaglio, F., and Bax, A. (1998) Measurement of J and dipolar couplings from simplified two-dimensional NMR spectra. *J. Magn. Reson. 131*, 373–378.
21. Salzmann, M., Pervushin, K., Wider, G., Senn, H., and Wuthrich, K. (1998) TROSY in triple-resonance experiments: new perspectives for sequential NMR assignment of large proteins. *Proc. Natl. Acad. Sci. U.S.A. 95*, 13585–13590.
22. Herrmann, T., Guntert, P., and Wuthrich, K. (2002) Protein NMR structure determination with automated NOE assignment using the new software CANDID and the torsion angle dynamics algorithm DYANA. *J. Mol. Biol. 319*, 209–227.
23. Banci, L., Bertini, I., Huber, J. G., Luchinat, C., and Rosato, A. (1998) Partial orientation of oxidized and reduced cytochrome b5 at high magnetic fields: Magnetic susceptibility anisotropy contributions and consequences for protein solution structure determination. *J. Am. Chem. Soc. 120*, 12903–12909.
24. Herrmann, T., Guntert, P., and Wuthrich, K. (2002) Protein NMR structure determination with automated NOE-identification in the NOESY spectra using the new software ATNOS. *J. Biomol. NMR 24*, 171–189.
25. Case, D. A., Darden, T. A., Cheatham, T. E., Simmerling, C. L., Wang, J., Duke, R. E., Luo, R., Merz, K. M., Wang, B., Pearlman, D. A., Crowley, M., Brozell, S., Tsui, V., Gohlke, H., Mongan, J., Hornak, V., Cui, G., Beroza, P., Schafmeister, C. E., Caldwell, J. W., Ross, W. S., Kollman, P. A. (2008) AMBER 10. [8.0], San Francisco, CA, University of California.
26. Laskowski, R. A., Rullmann, J. A. C., MacArthur, M. W., Kaptein, R., and Thornton, J. M. (1996) AQUA and PROCHECK-NMR: Programs for checking the quality of protein structures solved by NMR. *J. Biomol. NMR 8*, 477–486.
27. Bhattacharya, A., Tejero, R., and Montelione, G. T. (2007) Evaluating protein structures determined by structural genomics consortia. *Proteins 66*, 778–795.
28. Vriend, G. (1990) WHAT IF: A molecular modeling and drug design program. *J. Mol. Graphics 8*, 52–56.
29. Koradi, R., Billeter, M., and Wuthrich, K. (1996) MOLMOL: a program for display and analysis of macromolecular structure. *J. Mol. Graphics 14*, 51–55.
30. McGinnis, S., and Madden, T. L. (2004) BLAST: at the core of a powerful and diverse set of sequence analysis tools. *Nucleic Acids Res. 32*, W20–W25.
31. Thompson, J. D., Higgins, D. G., and Gibson, T. J. (1994) CLUSTAL W: improving the sensitivity of progressive multiple sequence alignment through sequence weighting, position-specific gap penalties and weight matrix choice. *Nucleic Acids Res. 22*, 4673–4680.
32. Sazinsky, M. H., Agarwal, S., Arguello, J. M., and Rosenzweig, A. C. (2006) Structure of the actuator domain from the *Archaeoglobus fulgidus* Cu(+)-ATPase. *Biochemistry 45*, 9949–9955.
33. Eswar, N., Webb, B., Marti-Renom, M. A., Madhusudhan, M. S., Eramian, D., Shen, M. Y., Pieper, U., Sali, A. (2007) Comparative protein structure modeling using MODELLER Curr. Protoc. Protein Sci. Chapter 2, Unit.
34. Farrow, N. A., Muhandiram, R., Singer, A. U., Pascal, S. M., Kay, C. M., Gish, G., Shoelson, S. E., Pawson, T., Forman-Kay, J. D., and Kay, L. E. (1994) Backbone dynamics of a free and phosphopeptide-complexed Src homology 2 domain studied by $^{15}N$ NMR relaxation. *Biochemistry 33*, 5984–6003.

35. Grzesiek, S., and Bax, A. (1993) The importance of not saturating $H_2O$ in protein NMR. Application to sensitivity enhancement and NOE measurements. *J. Am. Chem. Soc. 115*, 12593–12594.
36. Mandel, M. A., Akke, M., and Palmer, A. G.III (1995) Backbone dynamics of *Escherichia coli* ribonuclease HI: correlations with structure and function in an active enzyme. *J. Mol. Biol. 246*, 144–163.
37. Lipari, G., and Szabo, A. (1982) Model-Free approach to the interpretation of nuclear magnetic resonance relaxation in macromolecules. 1. Theory and range of validity. *J. Am. Chem. Soc. 104*, 4546–4559.
38. Lipari, G., and Szabo, A. (1982) Model-free approach to the interpretation of nuclear magnetic resonance relaxation in macromolecules. 2. Analysis of experimental results. *J. Am. Chem. Soc. 104*, 4559–4570.
39. Golovanov, A. P., Hautbergue, G. M., Wilson, S. A., and Lian, L. Y. (2004) A simple method for improving protein solubility and long-term stability. *J. Am. Chem. Soc. 126*, 8933–8939.
40. Garcia, d. l. T., Huertas, M. L., and Carrasco, B. (2000) HYDRONMR: prediction of NMR relaxation of globular proteins from atomic-level structures and hydrodynamic calculations. *J. Magn. Reson. 147*, 138–146.
41. Wishart, D. S., and Sykes, B. D. (1994) Chemical shifts as a tool for structure determination. *Methods Enzymol. 239*, 363–392.
42. Laskowski, R. A., MacArthur, M. W., Moss, D. S., and Thornton, J. M. (1993) PROCHECK: a program to check the stereochemical quality of protein structures. *J. Appl. Crystallogr. 26*, 283–291.
43. Wu, C. C., Rice, W. J., and Stokes, D. L. (2008) Structure of a copper pump suggests a regulatory role for its metal-binding domain. *Structure. 16*, 976–985.
44. Lutsenko, S., Barnes, N. L., Bartee, M. Y., and Dmitriev, O. Y. (2007) Function and regulation of human copper-transporting ATPases. *Physiol Rev. 87*, 1011–1046.
45. Olesen, C., Sorensen, T. L., Nielsen, R. C., Moller, J. V., and Nissen, P. (2004) Dephosphorylation of the calcium pump coupled to counterion occlusion. *Science 306*, 2251–2255.
46. Toyoshima, C., and Nomura, H. (2002) Structural changes in the calcium pump accompanying the dissociation of calcium. *Nature 418*, 605–611.
47. Lubben, M., Portmann, R., Kock, G., Stoll, R., Young, M. M., and Solioz, M. (2009) Structural model of the CopA copper ATPase of Enterococcus hirae based on chemical cross-linking. *Biometals 22*, 363–375.
48. Toyoshima, C., and Mizutani, T. (2004) Crystal structure of the calcium pump with a bound ATP analogue. *Nature 430*, 529–535.
49. Toyoshima, C., Nakasako, M., Nomura, H., and Ogawa, H. (2000) Crystal structure of the calcium pump of sarcoplasmic reticulum at 2.6 Å resolution. *Nature 405*, 647–655.
50. Hatori, Y., Majima, E., Tsuda, T., and Toyoshima, C. (2007) Domain organization and movements in heavy metal ion pumps: papain digestion of CopA, a Cu+-transporting ATPase. *J. Biol. Chem. 282*, 25213–25221.